

## Article

# Experimental Investigation and Computational Fluid Dynamic Simulation of Hydrodynamics of Liquid–Solid Fluidized Beds

Amer A. Abdulrahman <sup>1</sup>, Omar S. Mahdy <sup>1</sup>, Laith S. Sabri <sup>1,2,\*</sup>, Abbas J. Sultan <sup>1,2</sup>, Hayder Al-Naseri <sup>2,3</sup>, Zahraa W. Hasan <sup>1</sup>, Hasan Shakir Majdi <sup>4</sup> and Jamal M. Ali <sup>1</sup>

<sup>1</sup> Chemical Engineering Department, University of Technology, Baghdad 10066, Iraq; amer.a.abdulrahman@uotechnology.edu.iq (A.A.A.); omar.s.mahdy@uotechnology.edu.iq (O.S.M.); ajshw9@umsystem.edu (A.J.S.); che.19.07@grad.uotechnology.edu.iq (Z.W.H.); jamal.m.ali@uotechnology.edu.iq (J.M.A.)

<sup>2</sup> Multiphase Flow and Reactors Engineering and Application Laboratory (mReal), Chemical and Biochemical Engineering Department, Missouri University of Science and Technology, Rolla, MO 65409, USA; h.alnaseri@umsystem.edu

<sup>3</sup> Chemical Engineering Department, Tikrit University, Tikrit MMH4+876, Iraq

<sup>4</sup> Chemical and Petroleum Industries Engineering Department, Al-Mustaqbal University College, Hillah 51001, Iraq; dr.hasanshker@mustaqbal-college.edu.iq

\* Correspondence: lssf25@umsystem.edu

**Abstract:** The present study provides and examines an experimental and CFD simulation to predict and accurately quantify the individual phase holdup. The experimental findings demonstrated that the increase of solid beads has a significant influence on the ( $U_{mf}$ ), as comparatively small glass beads particles require a low ( $U_{mf}$ ) value, which tends to increase as the diameter of the beads increases. Besides that, the expansion ratio is proportional to the velocity of the liquid. Even though, the relationship becomes inversely proportional to the diameter of the beads. The liquid holdup was found to increase with increasing liquid velocity, however, the solid holdup decreased. The Eulerian–Eulerian granular multiphase flow technique was used to predict the overall performance of the liquid–solid fluidized beds (LSFBs). There was a good agreement between the experimental results and the dynamic properties of liquid–solid flows obtained from the CFD simulation, which will facilitate future simulation studies of liquid–solid fluidized beds. This work has further improved the understanding and knowledge of CFD simulation of such a system at different parameters. Furthermore, understanding the hydrodynamics features within the two-phase fluidization bed, as well as knowing the specific features, is essential for good system design, enabling the systems to perform more effectively.

**Keywords:** two-phase fluidization; pressure drop; phase holdups; CFD simulation



**Citation:** Abdulrahman, A.A.; Mahdy, O.S.; Sabri, L.S.; Sultan, A.J.; Al-Naseri, H.; Hasan, Z.W.; Majdi, H.S.; Ali, J.M. Experimental Investigation and Computational Fluid Dynamic Simulation of Hydrodynamics of Liquid–Solid Fluidized Beds. *ChemEngineering* **2022**, *6*, 37. <https://doi.org/10.3390/chemengineering6030037>

Academic Editor: Luis M. Gandía

Received: 1 March 2022

Accepted: 9 May 2022

Published: 12 May 2022

**Publisher's Note:** MDPI stays neutral with regard to jurisdictional claims in published maps and institutional affiliations.



**Copyright:** © 2022 by the authors. Licensee MDPI, Basel, Switzerland. This article is an open access article distributed under the terms and conditions of the Creative Commons Attribution (CC BY) license (<https://creativecommons.org/licenses/by/4.0/>).

## 1. Introduction

Liquid and solid fluidization have received a considerable amount of attention in recent years, since it has been used in a variety of industrial applications, such as granulation in the pharmaceutical industry, chlorination in the semiconductor industry, hydrometallurgy and food technology, biochemical processing, and water treatment [1,2]. (LSFBs) have several benefits, including a high heat transfer rate system, well-mixing, a large contacting surface area, and a high fluid/solid relative velocity [3]. Moreover, fluidization is the process of converting solid particles into liquids by allowing liquid to flow upward. Solid particles suspended in water have seemed to be “fluidized” [4–6]. LSFBs are essential and effective process equipment that operate at high fluid velocities while maintaining homogeneous particle distribution. The flow system is usually denoted as the homogeneous regime when the mass and heat transfer between the two phases occur with high rates and efficiency in the system. Due to the enormous efficient mixing processes, the two-phase

liquid–solid fluidized process, in which the liquid is used as a continuous liquid, has a broad array of applications. It also allows for efficient mass or energy transfers [7,8].

In recent decades, many investigations explained the liquid–solid fluidized process, however, the influence of different particle sizes experimentally and numerically was poorly addressed in the literature, Table 1 identifies the sources of experimental and numerical studies in the literature. For instance, Hussein Zbib [9] created a linked (CFD) and a discrete element method (DEM) model to investigate fluid–solid and solid–solid interactions in a 3D (LSFB). The Electrical Resistance Tomography (ERT) experimental approach validated the CFD-DEM model in which 4.74 percent disparity between simulations and experiments. The bed-average particle volume fraction was measured using ERT. Aghajani et al. [10] utilized liquid–solid fluidization as a hydrometallurgical process for heat transfer improvements in the desalination plant. Four types of particles with different properties were tested by Wang et al. [11] in a narrow rectangular fluidized bed equipped with a high-speed video. Calibration curves of these different particles were achieved by correlating the grayscale of the digital images with the corresponding solids holdup. Furthermore, in the work of Tang et al. [3], visual measurements were used to observe the expanded fluidization behavior in liquid–solid mini-fluidized beds (MFBs). The presence of wall effects in liquid–solid MFBs was identified and explained and found that a ratio of the solid particle diameter to the bed diameter varied from 0.017 to 0.091; the measured incipient/ $(U_{mf})$  in the MFBs was 1.67 to 5.25 times higher than that calculated using the Ergun equation. Furthermore, the ratio of the Richardson–Zaki (R–Z) exponent derived using the R–Z correlation to that obtained by fitting with experimental data ranged from 0.92 to 0.55. Additionally, several experiments were conducted by Mandal [8] to investigate the hydrodynamic properties of particles in a liquid–solid fluidized bed. Factors such as particle size, the percentage of interstitial void volume, and the temperature of the bed wall were examined. The results show that particles in a liquid–solid packed fluidized bed are lower ( $U_{mf}$ ) than those in a mono liquid–solid fluidized bed. In most cases, the solids bed is “fixed” or limited within a specific device in an immobile state. When a flowing medium generates the forces, solids are no longer fixed by mechanical constraints and are instead allowed to move freely. Both experiments and simulations were employed by Nijssen et al. [12] to gain insight into the heterogeneous behavior of drinking water softening reactors. According to literature, (LSFB) systems are often considered homogeneous at modest velocities. Nevertheless, local voids were observed in the experiments with calcite grains at relatively low fluid velocities and significant heterogeneous particle–fluid patterns at higher fluid velocities. Peng et al. [13] used an Eulerian–Eulerian two-phase model (kinetic theory of granular flow) to study the hydrodynamic characteristics and fluidization behaviors of the particles. CFD model was validated by comparing the experimental data and simulation results regarding the expansion degree of low and high density. A CFD-DEM simulation model was used, and its results were compared with expansion measurements and high-speed videos and images. Many numerical approaches have simulated the flow and hydrodynamics generation within LSFBs. Numerical analysis and modeling of fluidized processes have significantly and effectively contributed to estimating and understanding the complex hydrodynamics generated by two- or three-phase fluidization. CFD offers several approaches and models through which fluidization beds are studied, modeled, and analyzed. The most important techniques are the Eulerian–Lagrangian model, called the discrete particles model, and the Eulerian–Eulerian model called the granular flow model. The relationships between solid holdup ( $\varepsilon_S$ ) and liquid holdup ( $\varepsilon_L$ ) in a liquid–solid fluidized bed system are represented by the expressions Equations (1)–(3) [14]:

$$\varepsilon_S + \varepsilon_L = 1 \quad (1)$$

The solid holdup can be calculated using the following formula:

$$\varepsilon_S = M_s / \rho_S A_c H_e \quad (2)$$

where  $A_c$  represents the cross-sectional area of the column,  $H_e$  describes the expanded bed height, and  $M_s$  represents the solid mass of the column.

In the absence of frictional pressure drop, the static pressure gradient ( $\Delta P$ ) is defined as:

$$\Delta P/H_e = g (\rho_L \varepsilon_L + \rho_S \varepsilon_S) \quad (3)$$

Individual holdups can be calculated using Equations (1)–(3). In these equations, the bed height is measured visually. The ( $U_{mf}$ ) of the fluidized beds is an essential hydrodynamic property. It is necessary to design reactors or other contacting devices based on fluidized bed technology. That is because it represents the transition from the behavior of a solids-packed bed to the conduct of a fluidized bed. The ( $U_{mf}$ ) is determined experimentally by plotting the bed pressure drop against the liquid velocity. During fluidization, the pressure drop across the bed would no longer change with the increase in liquid flow rate. Thus, the ( $U_{mf}$ ) is equal to the flow rates at which a curve break occurs [15,16]. It is essential to mention that visual observations characterize the ( $U_{mf}$ ) as either the velocity at which the bed first begins to expand or the velocity at which every particle in the bed continually shifts position with adjacent particles [3]. Given Equation (4), the Ergun expression is used to calculate the ( $U_{mf}$ ).

$$U_{mf}^2 = \frac{\varnothing d_p (\rho_s - \rho_L)}{1.75 \rho_L} g \varepsilon_{mf}^3 \quad (4)$$

Previous investigations poorly investigated the influence of different particle sizes experimentally and numerically in liquid–solid fluidized beds. Therefore, the experimental analysis and simulation of hydrodynamics in LSFs using CFD techniques are the main objective of this research. Time-dependent simulations of liquid–solid two-phase flows are carried out using commercial software, FLUENT 4.5.6 (ANSYS Academic Research & Teaching Licenses). The effects of operating conditions and particle diameter on hydrodynamics are examined and compared to experimental data. The goal is to create a strong foundation for reactor simulation.

**Table 1.** Some of the sources of previous studies in a fluidized bed for experimental investigations and CFD simulation.

	Authors	Year	System	Solid Material	Measuring System	Key Findings
1	Jack T. Cornelissen, et al. [17]	2007	Liquid–Solid	Glass beads	Liquid–solid fluidization system	A liquid–solid fluidized bed is simulated using a multifluid Eulerian computational fluid dynamics (CFD) model with granular flow extension.
2	Md. Saifur Rahaman, et al. [18]	2017	Liquid–Solid	Polydisperse struvite crystals	A fluidized bed, built of Plexiglas with diameter 100 mm and height 1392 mm	The simulated bed expansion behavior of struvite crystals of various sizes was found to be consistent with experimental results. The six different size groups of struvite investigated in this study were found to be classified according to their sizes at steady state, with limited intermixing between successive layers.
3	Yupeng Xua, et al. [19]	2017	Gas–Solid	polyethylene (HDPE) particles	A small-scale full-loop circulating fluidized bed (CFB)	The effect of different drag laws used in CFD simulations is considered in this work through a detailed and direct comparison with experimental data from a small-scale, full-loop circulating fluidized bed.

Table 1. Cont.

	Authors	Year	System	Solid Material	Measuring System	Key Findings
4	Lipak Kumar Sahoo, et al. [20]	2021	Gas–Solid	Silica-gel beads	A two-dimensional gas–solid tapered fluidized bed	Using an image analysis method, the hydrodynamic behavior of tapered beds was investigated experimentally. The overlapping of binary images was used to quantify the peripheral unfluidized region.
5	Yusuf H. Bello, et al. [21]	2021	Gas–Solid	Silica sand	In a lab-scale fluidized bed reactor (FBR)	The size and number of air distributor orifices in a lab-scale fluidized bed reactor (FBR) are applied to enhance biomass conversion.

#### Classification of Particles for Liquid Fluidization

The principle for transformation from particulate to the aggregate performance of fluidized beds can be established in dimensionless formula according to Gibilaro et al. [22], represented by Equations (5) and (6).

$$\left(\frac{3 C_D D_e}{4(2 + D_e)}\right)^{0.5} - 0.4n(1 - \varepsilon)^{0.5} \varepsilon^{n-1} \times \alpha = \begin{cases} +ve, & \text{particulate} \\ 0, & \text{particulate and aggregate} \\ -ve, & \text{aggregate} \end{cases} \quad (5)$$

$$\alpha = \sqrt{1 + \left(\frac{3D_e}{2 + D_e}\right) \cdot \left(\frac{(1 - n(1 - \varepsilon))^2}{n^2 \varepsilon(1 - \varepsilon)}\right)} \quad (6)$$

For the dense fluidization bed, Equation (5) gives a satisfying prediction by comparing the predicted behavior and experimental results. Di-Felice [23] used Equation (5) to construct a flow map in dimensionless form for particles fluidized by any fluid.

## 2. Experimental Setup

The hydrodynamics and interaction between liquid and solid phases were studied experimentally. Furthermore, the effect of the superficial liquid velocity and solid particle diameter on the ( $U_{mf}$ ), pressure drop, bed expansion, and individual phase holdup in a fluidized bed column are investigated. As indicated in Figure 1, all experiments were carried out in a two-phase fluidization bed system. Glass beads of various sizes and uniform shapes with diameters of 0.003 m, 0.004 m, and 0.006 m and a density of 2500 kg/m<sup>3</sup> were used to represent solid-bed systems, with water as the liquid phase.

The scale of the experiments in this study is listed in Table 2. The fluidized column is formed by two essential parts: the test section and the liquid distributor box, which also support the glass beads.

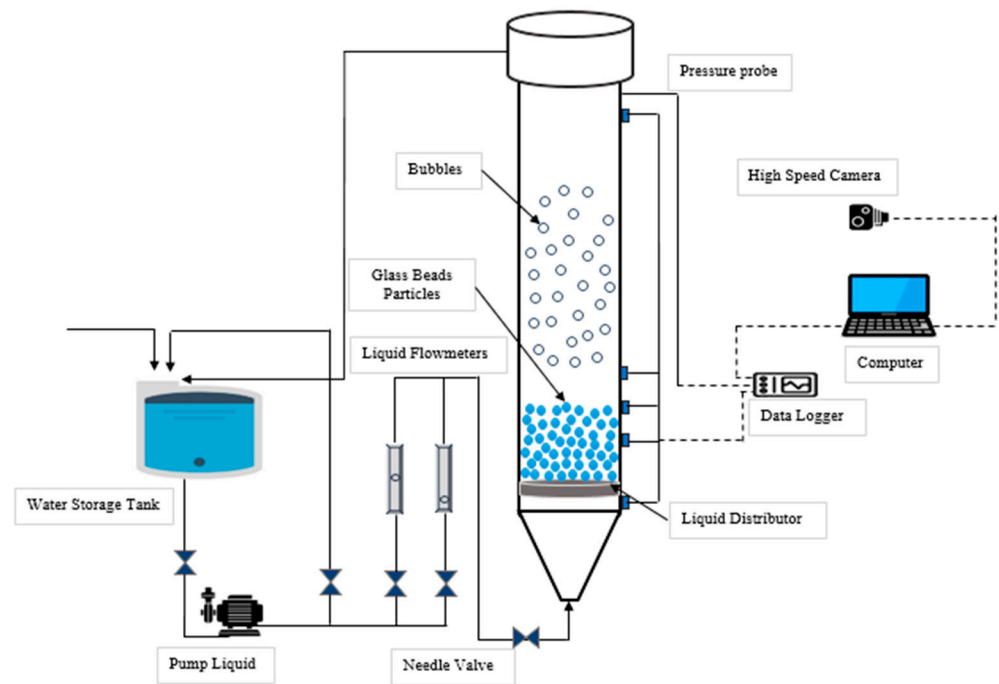


**Figure 1.** Schematic diagram of the experimental rig.

**Table 2.** The experimental data used in this investigation.

Materials	$d_p$ (m)	$\rho_s$ (kg/m <sup>3</sup> )	Initial Static Bed Height (m)
Properties of bed materials			
Glass beads	0.003	2500	0.12
Glass beads	0.004	2500	0.121
Glass beads	0.006	2500	0.126
Properties of medium fluidizing			
Materials	$\mu_L$ (pa s)	$\rho_s$ (kg/m <sup>3</sup> )	Superficial velocity (m/s)
Water at 30 °C	0.000891	997.15	0.0–0.1

The major component of the test unit, in which the fluidization process happens, is a vertical cylindrical Perspex column with an inner diameter of 0.115 m and a height of 1.7 m. The lowest part of the column has a distributor constructed of Perspex sheet with a thickness of 0.004 m. The distributor plate was designed using the orifice theory (Kunii) [17]. It was created to connect the two parts of the test section and support the beads of the bed. The plate was drilled with 274 holes, each with a diameter of 2 mm, to ensure that liquid flowed uniformly throughout the bed. Water is pumped into the test column via a pipe in the lower part of the column by a water pump with a capacity of 0.0015 m<sup>3</sup>/s and a maximum head of 30 m, connected to a 0.1 m<sup>3</sup> water tank. The water flow rate may be accurately controlled and measured using needle valve rotameters on the feed and bypass lines. In the current study, the pressure drop in the bed was measured using five Keller type PA 21Y/4 differential pressure transducers (KELLER AG Druckmesstechnik, Switzerland) placed at a specific interval up the column wall. Each pressure reading was recorded on a laptop. A pressure transducer is a novel device that converts pressure into an electrical signal. Ordeal model UDL 100 data loggers were utilized to convert analog signals to numerical values. The UDL 100 (Universal Design License) Model devices convert various analog signals used in industrial applications into digital values that can then be transmitted to a laptop. These devices have been configured on the laptop, and then the DALi 08 software is used to store device values and configure them on the laptop.

### 3. Computational Model

CFD is widely used in previous studies and process engineers to assess the flow and performance of process equipment [17,24–27]. Momentum transfer between particles and fluid is essential when simulating fluidized beds. Drag force and particle-phase rheology have been demonstrated to impact bed hydrodynamics in previous simulations of liquid–solid systems significantly. As a result, different drag force models are covered in the following section.

#### 3.1. Simulation Details

The simulation program ANSYS, version 2019.R1, was used in this study. The boundary layer meshed the boundary of the shapes. The rest of the geometry was auto meshed with schema called tetrahedral, triangular, and quadrilateral (QUAD) for 2D geometry involves simulation of two-phase fluidization phenomena types, as shown in Figure 2. The number of nodes is 73,400, and the number of elements is 72,568, with 1.35 mm.

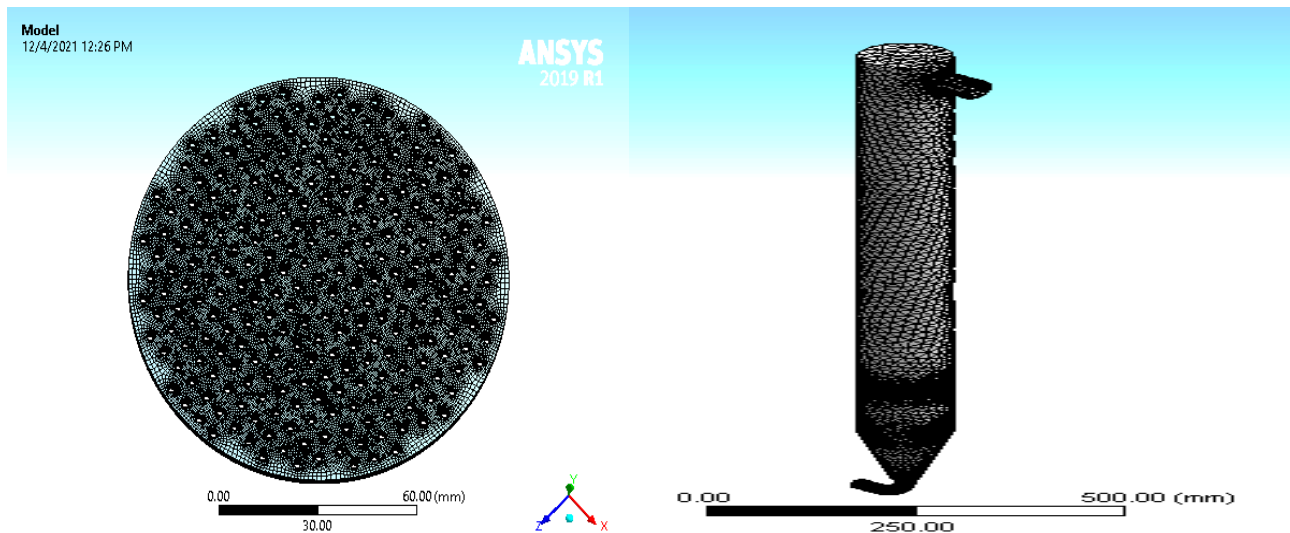


**Figure 2.** Two-dimensional computational geometry of a fluidized bed.

#### 3.2. Governing Equations

Governing equations signify the essential values of CFD. The conservation of mass or the continuity can be expressed as shown in Equation (7) [28,29]:

$$\frac{\partial \rho_L}{\partial t} + (\nabla \cdot \rho_f u) = 0 \quad (7)$$

For incompressible fluids (Newtonian), the conservation of momentum expression can be written as the Navier–Stokes Equation (8) [29,30]:

$$\rho_L \left( \frac{\partial u}{\partial t} + u \cdot \nabla u \right) = (-\nabla p) + \mu_L \nabla^2 + \rho_L g \quad (8)$$

To solve the Navier–Stokes equations, it needs a perfect description of the boundary conditions. There are several boundary conditions in fluid mechanics which are frequently used [29].

#### 3.3. Drag Models

The dynamic force for fluidization is generated mainly from the drag force [31]. Many experimental relationships and computer model methods were established to define the particle–fluid drag force. These are generally known as “drag models”. Some are based on bed pressure drop or bed expansion experiments, such as the Zaki–Richardson drag

model [32]. Other models depend on Lattice–Boltzmann computer simulations, such as the Hill Koch Ladd model [33]. The following Syamlal and O'Brien [34] drag is the drag model used in this study.

The Syamlal–O'Brien drag model can be expressed as shown in Equations (9)–(13)

$$\beta_{pL} = \frac{3 \epsilon_s \epsilon_L \rho_L}{4 v_t^2 d_p} C_D \left( \frac{Re_p}{v_t} \right) |u - v| \quad (9)$$

$$C_D = \left( 0.63 + \frac{4.8}{\sqrt{\frac{Re_p}{v_t}}} \right)^2 \quad (10)$$

$$v_t = 0.5 \left( A - 0.06 Re_p + \sqrt{(0.06 Re_p)^2 + 0.12 Re_p (2B - A) + A^2} \right) \quad (11)$$

where  $A$  and  $B$  are a function of  $\epsilon_f$ .

$$A = \epsilon_L^{4.14}, \quad B = 0.8 \epsilon_L^{4.14}, \quad \epsilon_L \leq 0.85 \quad (12)$$

$$A = \epsilon_L^{4.14}, \quad B = \epsilon_L^{2.65}, \quad \epsilon_L > 0.85 \quad (13)$$

and particle Reynolds number ( $Re_p$ ) can be expressed as:

$$Re_p = \rho_L u_L d_p / \mu_L \quad (14)$$

#### 4. Discussion

Experiments with a fluidized bed of water–glass beads have been carried out with varying liquid velocities and particle sizes, and the results are graphically represented.

##### 4.1. Bed Pressure Drop and Minimum Fluidization Velocity ( $U_{mf}$ )

Pressure drop in the fluidized bed was measured in this study using a pressure transducer linked to Ordeal model UDL 100 data loggers, as detailed in Section 2. All of the experiments began with the column filled with water and glass beads, which had been raised to the necessary height. The rate of liquid flow was increased gradually. It has been observed that the pressure drop at the bed shows two behaviors for two phases (water–solid): The first point, due to the fluidization process, bed pressure drop was strongly influenced by superficial water velocity, and bed pressure drop rose as superficial water velocity increased. The second point is that once the bed has been fluidized, the pressure drop continues to stabilize without being affected by an increase in the superficial water velocity [19,35,36]. When fluid is forced through the glass beads bed, the beads remain static, causing more pressure to be lost by allowing the bed particles to fluidize. The pressure drop becomes constant because the fluid (liquid) resistance decreases as the bed fluidizes. Figure 3 shows the relationship between pressure drop and liquid velocity for various particle sizes.

The pressure drop increase as the diameter of glass beads increases; this is because the pressure drops required counterbalancing the weight of the bed particles increase as the diameter of the beads increases. Figure 4 shows the relationship between different particle sizes and ( $U_{mf}$ ).

The ( $U_{mf}$ ) increases as the particle size increases, starting at 0.0385 m/s for granules with a diameter of 3 mm and increasing to 0.0417 m/s, 0.061 m/s for particles with a diameter of 4 and 6 mm, respectively. As shown in Figures 3 and 4, the pressure drop increases as the diameter of glass beads increases; this is because the pressure drops required to counterbalance the weight of the bed particles increases as the diameter of the beads increases. Thus, the ( $U_{mf}$ ) increased as the diameter of the particles increased.

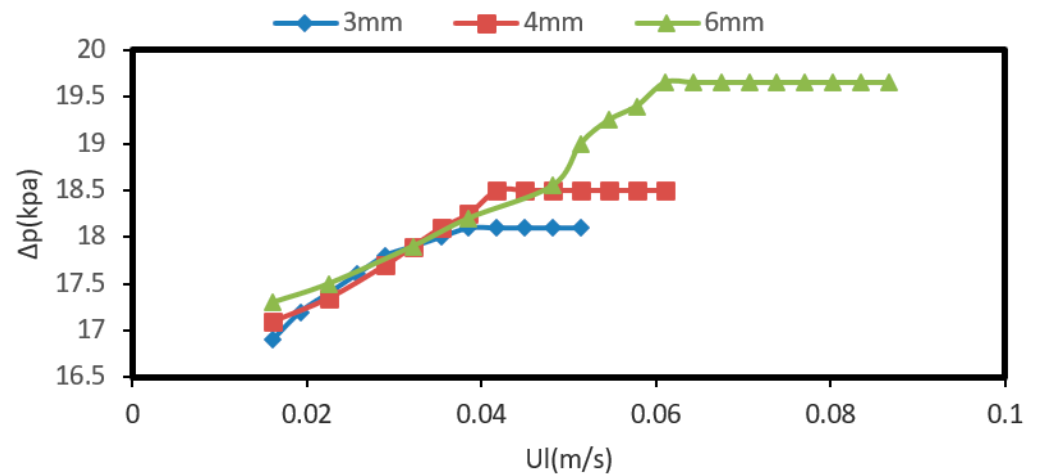


**Figure 3.** Variation of pressure drop with liquid velocity for different particle diameters.

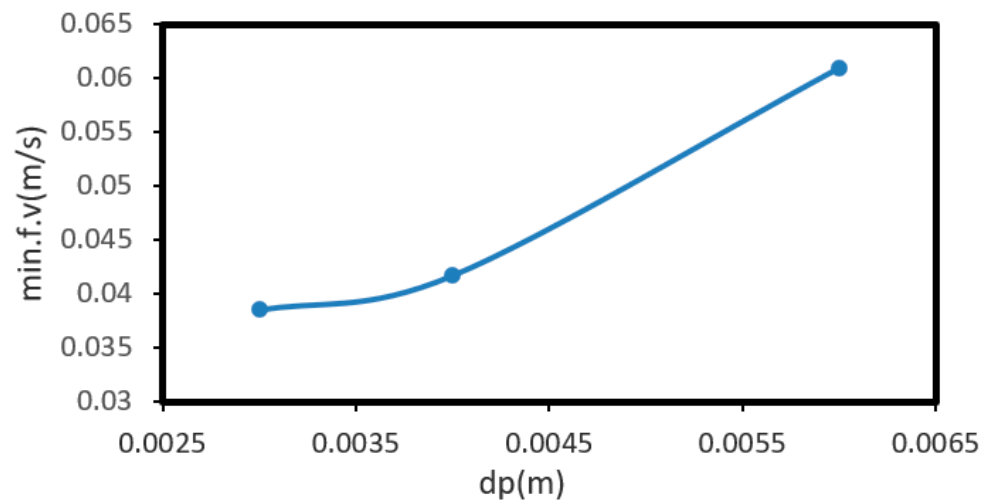


**Figure 4.** Variation of minimum fluidization velocity with different particle diameters.

#### 4.2. Bed Expansion

The fluidized bed height to the static bed height ratio is the bed expansion ratio ( $R$ ). When it regards system sizing, knowing the expanded bed height is important [37–40]. This work determined the bed expansion ratio using visual inspection when dealing with the two-phase flow (liquid–solid). Figure 5 shows the variation of bed expansion ratio and liquid velocity concerning particle diameter.

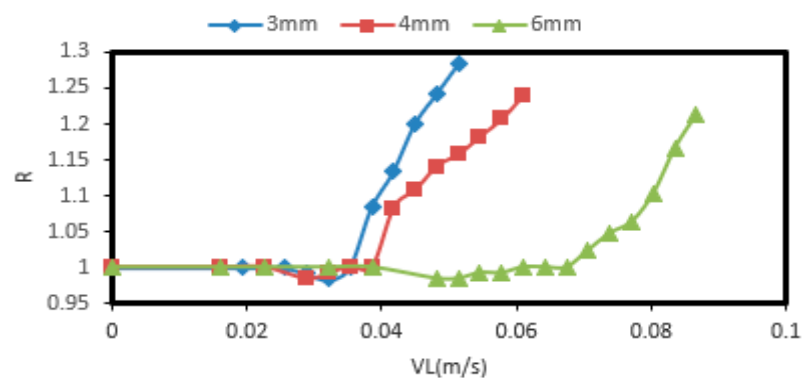


**Figure 5.** Variation of bed expansion ratio with liquid velocity for various particle diameters.

The bed remained static as the water velocity increased until it reached the ( $U_{mf}$ ). According to the statement, as particle diameter increases, the ( $U_{mf}$ ) increases, and thus the bed expansion ratio increases as the liquid velocity for a given particle diameter increases. As particle diameter rose, the bed expansion ratio decreased. This is due to the high specific weight of large-diameter particles.

#### 4.3. Phase Holdup

In a multiphase system, the phase holdup is described as the volume fraction occupied by the system phase considered [41–44].

##### 4.3.1. Solid Holdup

Equation (2) was used to calculate the solid holdup values. Figure 5 shows these results for various particle diameters.

It can be seen in this Figure that the relationship between liquid velocity and solid holdups remained constant from fixed bed to ( $U_{mf}$ ) and then steadily decreased as the fluidizing velocity increased. Furthermore, before ( $U_{mf}$ ), there was no numerical variation in solid holdup for different particle diameters because solid holdup is completely dependent on the height of bed particles. The bed expands as the superficial liquid velocity increases; the liquid holdups increase, resulting in a decrease in the solid holdup in the bed. The solid holdup in the beds of the particles (3 mm) is slightly higher than that of other glass beads particles, as shown in Figure 6. Due to the buoyancy forces acting on the particles, it is well known that relatively light particle beds can easily expand in two-phase fluidized beds [21,45].

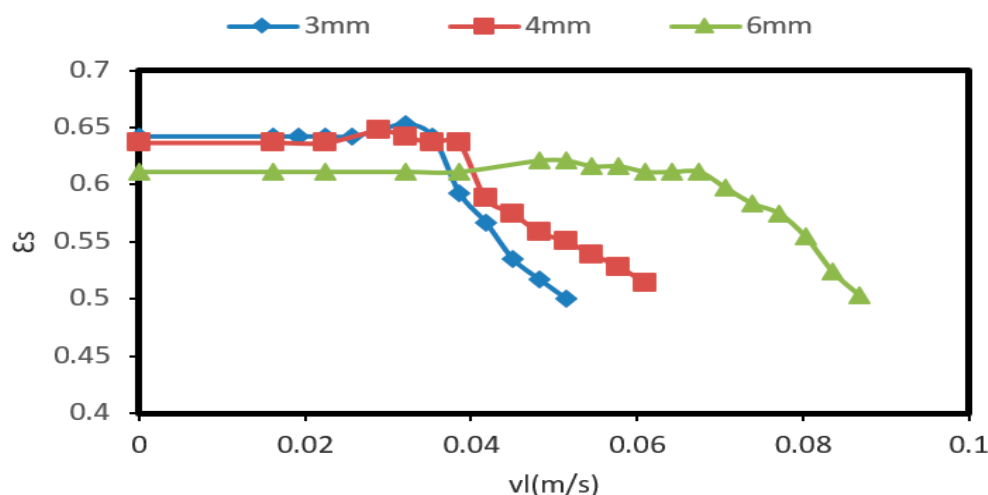


**Figure 6.** Variation solid holdup with liquid velocity for various particle diameters.

##### 4.3.2. Liquid Holdup

The values of solid holdup were calculated from Equation (1). The variation in fraction liquid holdup and liquid velocity for various particle diameters is represented in Figure 7.

The figure shows that liquid holdup remained constant until ( $U_{mf}$ ) and increased after ( $U_{mf}$ ) with increasing liquid velocity for all particles. Since the volume of liquid pumped into the riser increases [46,47], this increases the liquid velocity that increases liquid volume throughout the bed and expansion of the bed, resulting in an increase in the liquid holdup in the bed.

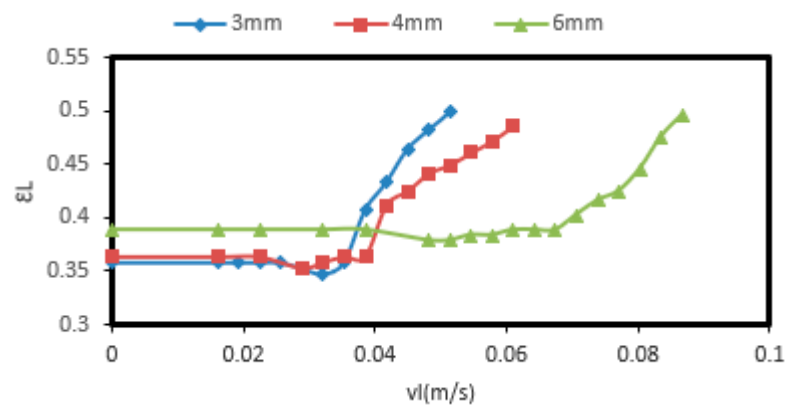


**Figure 7.** Variation liquid holdup with liquid velocity for various particle diameters.

#### 4.4. CFD Simulation Results

The CFD simulations were performed under the transient model for 10 s, the time step size was 0.001 s and the number of time steps was 10,000. The Eulerian multiphase model was used to represent the two-phase fluidization bed. The liquid velocity was constant for all case studies with 0.16 m/s, and the glass beads' diameters were 3 mm, 4 mm, and 6 mm, and a constant density of 2500 kg/m<sup>3</sup>; the fluidization phenomenon occurs under different ( $U_{mf}$ ) as a result of the effect of drag forces applied on the glass beads.

##### 4.4.1. Particle Volume Fraction

Figure 8 shows the particle volume fraction at a different time of the fluidization process for a particle diameter of 3 mm. The effect of the water flow velocity on the behavior of the solid particles and the phenomenon of fluidization can be observed.

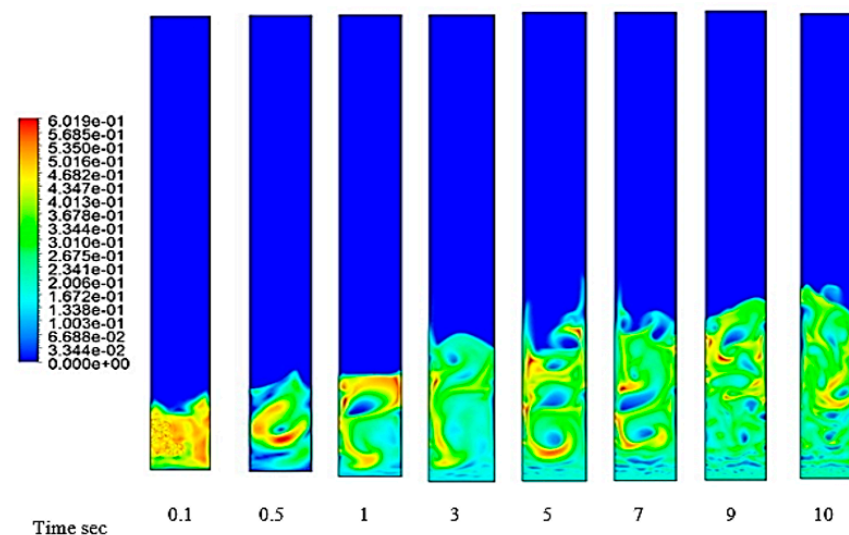


**Figure 8.** The volume fraction of particles diameter of 3 mm with different times.

Since a state of equilibrium is attained between the buoyant forces induced by increasing water flow and the gravitational forces that operate to keep the solid particles stable and fixed. As the velocity of the water increases, the buoyant forces overcome the gravitational forces, and the solid particles begin to move with the fluid and gain the same speed and direction of flow as the fluid, the particles start to rise through the fluidization column. Due to the impact of gravity's direction, the solid particles were not compelled to rise to the top, despite the physical fact that velocity reduces with increasing height. The velocity of the particles becomes minimal, causing them to fall to the bottom, and this process occurs regularly, resulting in the repetition of the process of rising and falling the

solid particles continuously with the flow of water. Figures 9 and 10 show the volume fraction of glass particles of diameters 4 and 6 mm, respectively. The effect of particles diameter is observable as the diameter of the particles increases the volume expansion decreases, so there is less volume expansion involved with 6 mm beads particles [48,49].

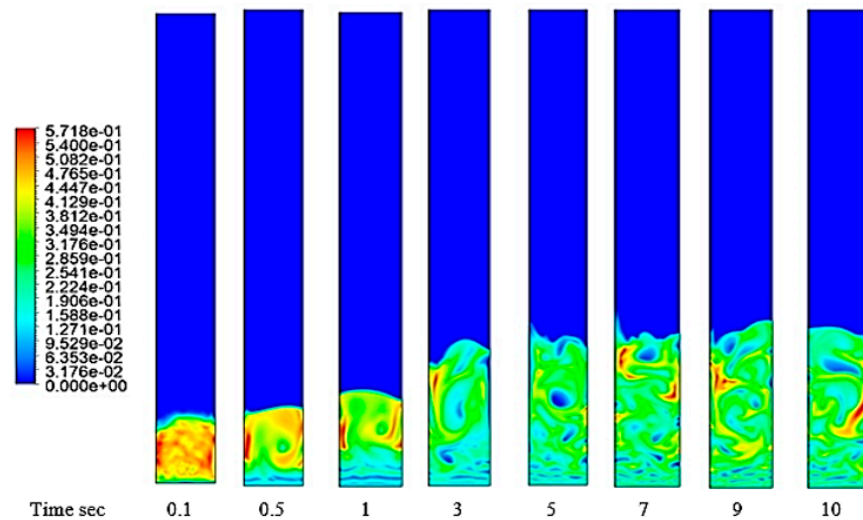


**Figure 9.** The volume fraction of particles with a diameter of 4 mm with different times.

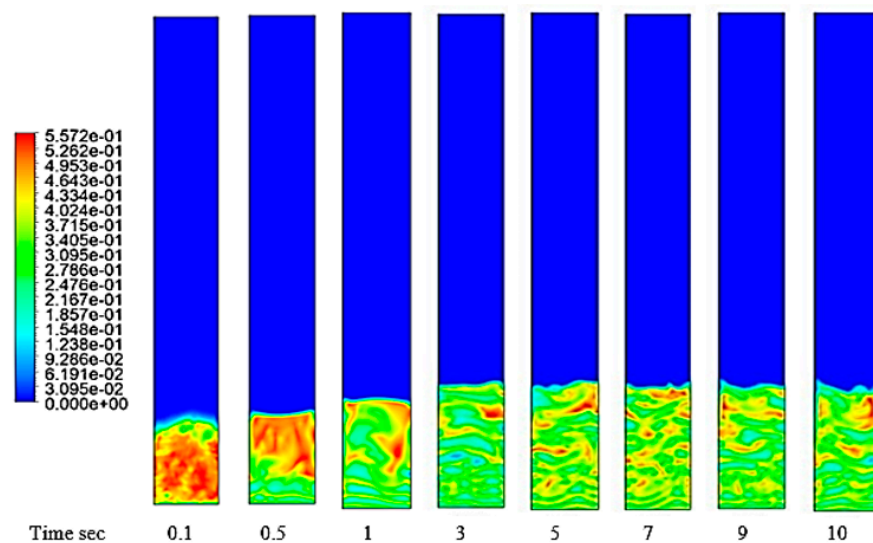


**Figure 10.** The volume fraction of particles with a diameter of 6 mm with different times.

The performance of the proposed CFD mathematical model was validated by comparing with the experimental data and the CFD simulation results in terms of the solid holdup. Figures 11–13 present variations of the solid holdup with superficial liquid velocity for particle diameters 3, 4, and 6 mm, respectively. In Figures 11 and 12 when the superficial liquid velocity increased from 0.032 m/s for the particle diameters 3 and 4 mm, the solid holdup decreased, while in Figure 13 when the superficial liquid velocity increased from 0.055 m/s for the particle diameter 6 mm, the solid holdup decreased. As can be seen from Figures 11–13, the CFD simulation results are in good agreement with the experimental data.

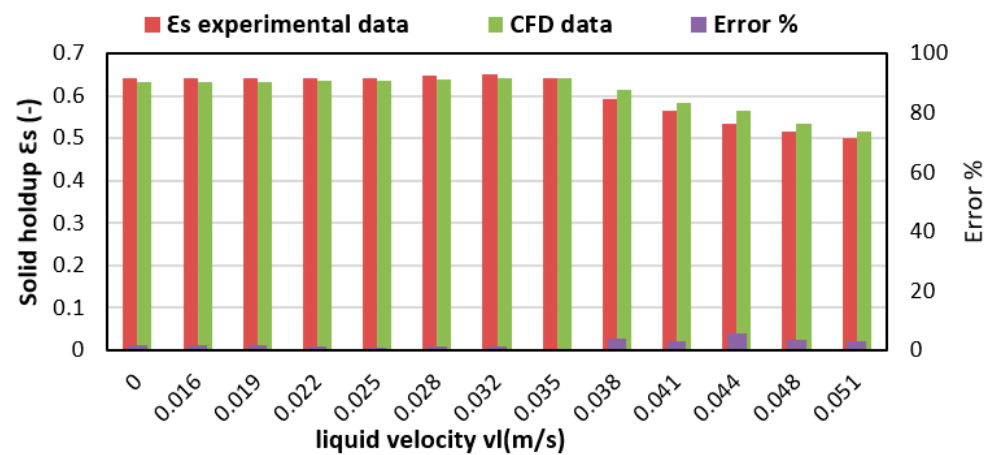


**Figure 11.** Comparisons between CFD simulation results and experimental data of solid holdup for particles with a diameter of 3 mm for different superficial liquid velocities.

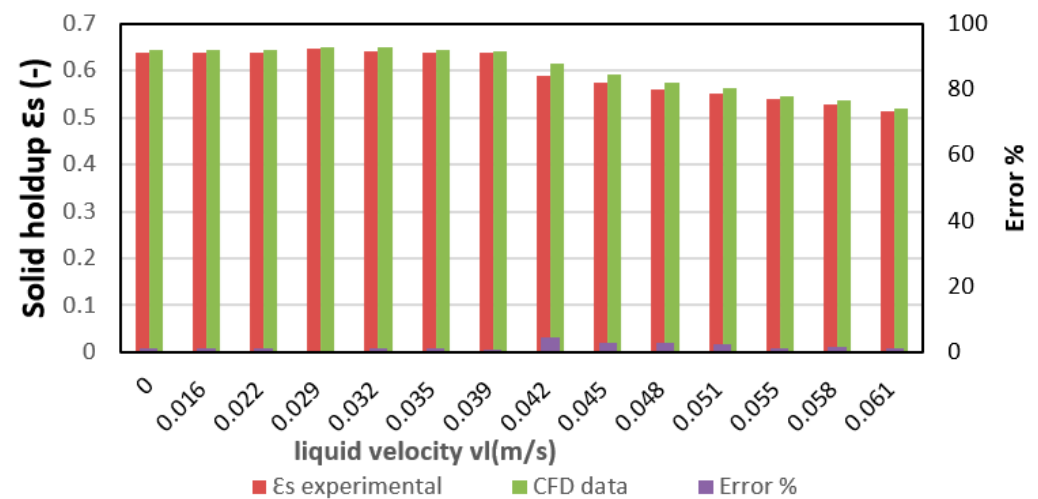


**Figure 12.** Comparisons between CFD simulation results and experimental data of solid holdup for particles with a diameter of 4 mm for different superficial liquid velocities.

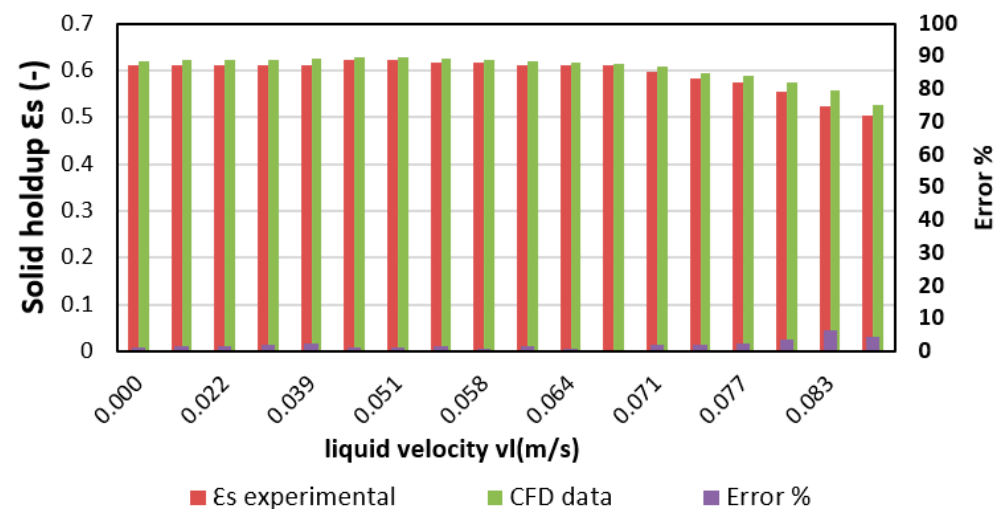


**Figure 13.** Comparisons between CFD simulation results and experimental data of solid holdup for particles with a diameter of 6 mm for different superficial liquid velocities.

#### 4.4.2. Particle Velocity

Figure 14 shows the velocity contours of particles of 3 mm diameter. It is noteworthy that the velocity of the particle varied with time.

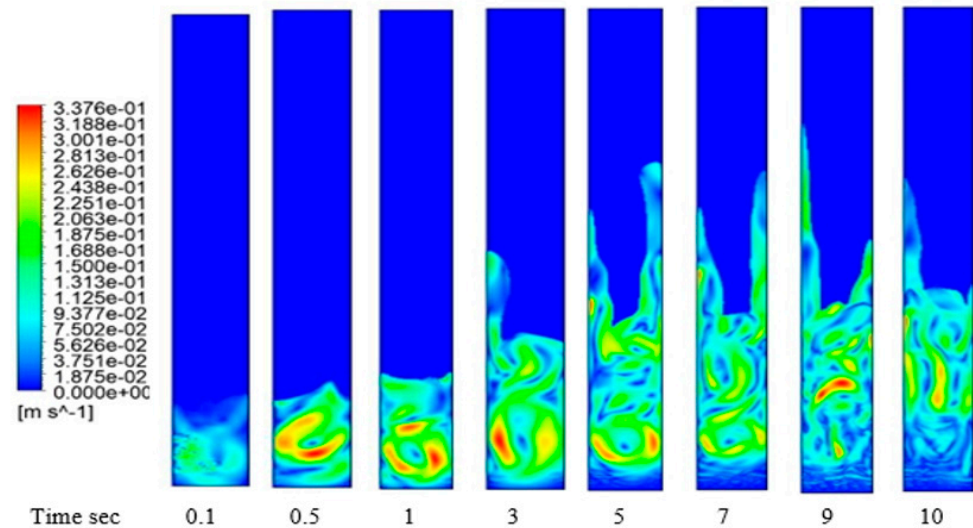


Figure 14. The velocity contour of particles with a diameter of 3 mm with time.

As shown in Figure 14, at a time of 0.1 s, the highest particle velocity occurs as a high-pressure drop. This is because the particles just started to be in dynamic conditions. After all, the liquid velocity reaches the ( $U_{mf}$ ). Bed heights increase as particles move upward with the flow direction until it reaches a certain height. Then the particles move down and return upward again until the bed height rests at a certain height. Figures 15 and 16 show the velocity contours of particles at diameters 4 mm and 6 mm, respectively.

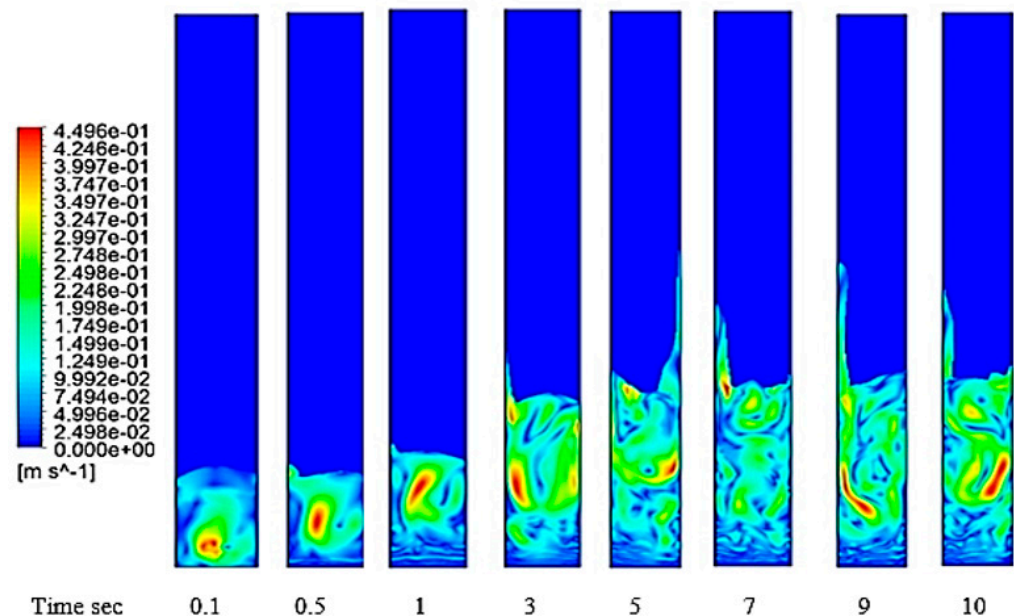


Figure 15. The velocity contour of particles with a diameter of 4 mm with time.

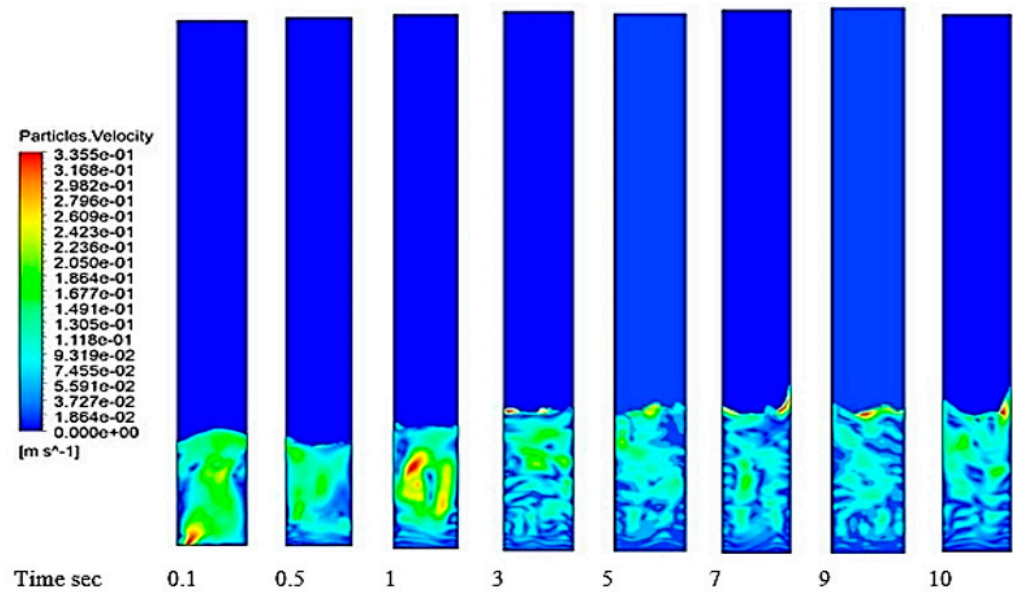


Figure 16. The velocity contour of particles with a diameter of 6 mm with time.

The effect of particle diameter is observed in Figure 17. The bed expansion affects the particle’s diameter. Therefore the particles with a diameter of 3 mm have the most significant bed expansion than other diameters. Furthermore, it can be noted that the particles with a diameter of 4 mm are more with the fluidization process. Figure 17 shows the velocity vectors of particles with 4 mm. It can be seen that the velocity vectors give a good and understanding explanation for particles behaving with time.

The particles were subjected to the drag force and acted like a liquid flow with an increase in the drag force. The gravity forces the particles to move upward at the first of the fluidization phenomenon until the liquid velocity decreases as its direction is opposite to gravity. Then the particles move downward, many collisions occur between particles as they interact. Thus, eddy formation considers a consequence of the fluidization process, which leads to an enhancement mixing process [49,50].

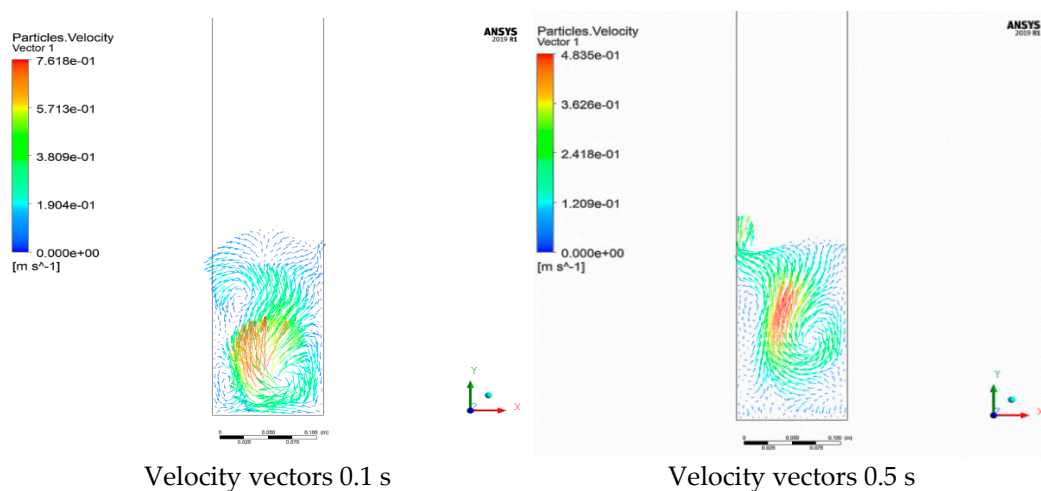
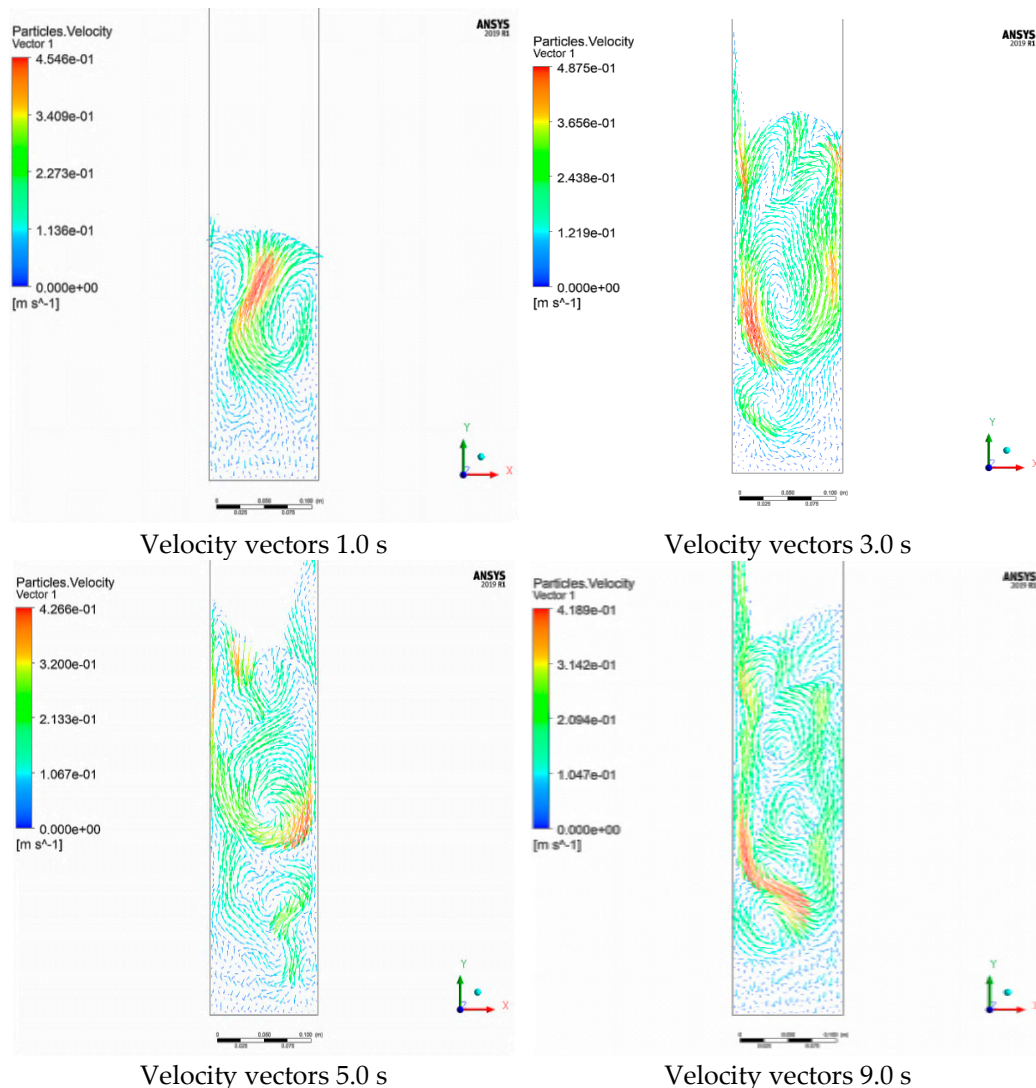


Figure 17. Cont.



**Figure 17.** The velocity vectors of particles diameter of 4 mm with time.

## 5. Conclusions

The hydrodynamic properties of a two-phase fluidized bed with different solid particle sizes were investigated through experiments. The key findings from the experimental results are summarized in the following:

The pressure drop across the bed increases as the liquid velocity increases before reaching the ( $U_{mf}$ ). After fluidization, the pressure drop is generally unaffected by the rise in water velocity and remains stable.

The particle size has a significant impact on the pressure drop and ( $U_{mf}$ ); as the particle size increases, thus increases the pressure drop and the ( $U_{mf}$ ).

The expansion ratio has a significant relation with liquid velocity and an inverse relationship with particle size. Therefore, the liquid holdup maintains a direct linear form with liquid velocity.

Furthermore, increasing the liquid velocity resulted in a higher liquid holdup.

The numerical solution provides a good prediction of how particles and fluid behave during the fluidization process and facilitates the development of a good fluidization column design.

**Author Contributions:** Conceptualization, L.S.S., A.A.A. and O.S.M.; methodology, L.S.S., A.J.S.; software, L.S.S., A.J.S. and H.A.-N.; validation, L.S.S., A.J.S., A.A.A. and O.S.M.; formal analysis, L.S.S., A.J.S.; investigation, L.S.S., A.J.S.; resources, L.S.S., A.J.S.; data curation, L.S.S., A.J.S., Z.W.H., A.A.A. and O.S.M.; writing—original draft preparation, L.S.S. and A.J.S.; writing—review and editing, L.S.S. and A.J.S.; visualization, L.S.S., J.M.A. and A.J.S.; supervision; project administration, L.S.S. and A.J.S.; funding acquisition, H.S.M. All authors have read and agreed to the published version of the manuscript.

**Funding:** This research received no external funding.

**Acknowledgments:** The authors would like to acknowledge the financial aid provided by Al-Mustaqbal University College, Ministry of Higher Education Iraq and the Higher Committee for Education Development in Iraq (HCED).

**Conflicts of Interest:** The authors declare no conflict of interest.

## Nomenclature

### Symbols Used

$A_C$	$m^2$	Cross-sectional area of the column
$C_D$	–	Drag reduction
CFD	–	Computational fluid dynamics
$d_p$	m	Particle diameter
$De$	–	Density number, $(\rho_f/\rho_s)$
$g$	$m/s^2$	Gravitational acceleration
$H_e$	m	Expanded bed height
$M_s$	kg	Mass of solid phase
$N$	–	Richardson and Zaki exponent
$\Delta P$	kpa	Pressure drop throughout the bed
$t$	s	Time
$u_L$	m/s	Liquid velocity
$u_{mf}$	m/s	Minimum fluidization velocity
$u_t$	m/s	Terminal velocity
Greek Letters		
$\beta_{pf}$	–	Bed expansion ratio
$\rho_L$	$kg/m^3$	Density of liquid
$\rho_S$	$kg/m^3$	Density of solid
$\varepsilon$	–	Holdup
$\varepsilon_L$	–	Liquid holdup
$\varepsilon_s$	–	Solid holdup
$\mu_L$	$Ns/m^2$	Liquid viscosity
$\emptyset$	–	Sphericity of the solid particle
$A$	–	Volume fraction in the liquid–nanoparticles suspension

## References

- Ehsani, M.; Movahedirad, S.; Shahhosseini, S. The effect of particle properties on the heat transfer characteristics of a liquid–solid fluidized bed heat exchanger. *Int. J. Therm. Sci.* **2016**, *102*, 111–121. [[CrossRef](#)]
- Jabir Shanshool, L.S.S. Removal of Phenol Pollutants by Modification Molecular Sieves 13X. *Eng. Technol. J.* **2009**, *27*, 2853–2862.
- Tang, C.; Liu, M.; Li, Y. Experimental investigation of hydrodynamics of liquid–solid mini-fluidized beds. *Particuology* **2016**, *27*, 102–109. [[CrossRef](#)]
- Sin, E.M.L.; Lim, E.W.C. Heat transfer from immersed tubes in a pulsating fluidized bed. *Powder Technol.* **2018**, *327*, 500–511. [[CrossRef](#)]
- Piemjaiswang, R.; Charoenchaipet, J.; Saelau, T.; Piumsomboon, P.; Chalermmsinuwana, B. Effect of design parameters on system mixing for a micro fluidized bed reactor using computational fluid dynamics simulation. *Braz. J. Chem. Eng.* **2020**, *38*, 21–31. [[CrossRef](#)]
- Wang, C.; Zhu, J. Developments in the understanding of gas–solid contact efficiency in the circulating fluidized bed riser reactor: A review. *Chin. J. Chem. Eng.* **2016**, *24*, 53–62. [[CrossRef](#)]
- Esteghamatian, A.; Hammouti, A.; Lance, M.; Wachs, A. Particle resolved simulations of liquid/solid and gas/solid fluidized beds. *Phys. Fluids* **2017**, *29*, 033302. [[CrossRef](#)]

8. Mandal, D. Hydrodynamics of particles in liquid–solid packed fluidized bed. *Powder Technol.* **2015**, *276*, 18–25. [[CrossRef](#)]
9. Zbib, H.; Ebrahimi, M.; Ein-Mozaffari, F.; Lohi, A. Hydrodynamic Behavior of a 3-D Liquid–Solid Fluidized Bed Operating in the Intermediate Flow Regime—Application of Stability Analysis, Coupled CFD-DEM, and Tomography. *Ind. Eng. Chem. Res.* **2018**, *57*, 16944–16957. [[CrossRef](#)]
10. Aghajani, M.; Müller-Steinhagen, H.; Jamialahmadi, M. New design equations for liquid/solid fluidized bed heat exchangers. *Int. J. Heat Mass Transf.* **2005**, *48*, 317–329. [[CrossRef](#)]
11. Wang, C.; Li, Z.; Wei, J.; Lan, X.; Ye, M.; Gao, J. Quantitative Measurement of Solids Holdup for Group A and B Particles Using Images and Its Application in Fluidized Bed Reactors. *Processes* **2022**, *10*, 610. [[CrossRef](#)]
12. Nijssen, T.; Kramer, O.; de Moel, P.; Rahman, J.; Kroon, J.; Berhanu, P.; Boek, E.; Buist, K.; van der Hoek, J.; Padding, J.; et al. Experimental and numerical insights into heterogeneous liquid-solid behaviour in drinking water softening reactors. *Chem. Eng. Sci.* **2021**, *11*, 100100. [[CrossRef](#)]
13. Peng, J.; Sun, W.; Han, H.; Xie, L. CFD Modeling and Simulation of the Hydrodynamics Characteristics of Coarse Coal Particles in a 3D Liquid-Solid Fluidized Bed. *Minerals* **2021**, *11*, 569. [[CrossRef](#)]
14. Singh, R.I.; Brink, A.; Hupa, M. CFD modeling to study fluidized bed combustion and gasification. *Appl. Therm. Eng.* **2013**, *52*, 585–614. [[CrossRef](#)]
15. Kaza, S.R.V.N. Effect of the Shape of the Baffles on the Hydrodynamics of a Fluidized Bed. *Int. J. Chem. React. Eng.* **2008**, *6*, 1–14. [[CrossRef](#)]
16. Sippola, P.; Kolehmainen, J.; Ozel, A.; Liu, X.; Saarenrinne, P.; Sundaresan, S. Experimental and numerical study of wall layer development in a tribocharged fluidized bed. *J. Fluid Mech.* **2018**, *849*, 860–884. [[CrossRef](#)]
17. Cornelissen, J.T.; Taghipour, F.; Escudí, R.; Ellis, N.; Grace, J.R. CFD modelling of a liquid–solid fluidized bed. *Chem. Eng. Sci.* **2007**, *62*, 6334–6348. [[CrossRef](#)]
18. Rahaman, S.; Choudhury, M.R.; Ramamurthy, A.S.; Mavinic, D.S.; Ellis, N.; Taghipour, F. CFD modeling of liquid-solid fluidized beds of polydisperse struvite crystals. *Int. J. Multiph. Flow* **2018**, *99*, 48–61. [[CrossRef](#)]
19. Xu, Y.; Musser, J.; Li, T.; Gopalan, B.; Panday, R.; Tucker, J.; Breault, G.; Clarke, M.A.; Rogers, W.A. Numerical Simulation and Experimental Study of the Gas–Solid Flow Behavior Inside a Full-Loop Circulating Fluidized Bed: Evaluation of Different Drag Models. *Ind. Eng. Chem. Res.* **2018**, *57*, 740–750. [[CrossRef](#)]
20. Sahoo, L.K.; Sarkar, S. Experimental Study of Bubble Behavior in a Two-Dimensional Gas–Solid Tapered Fluidized Bed. *Ind. Eng. Chem. Res.* **2021**, *60*, 12740–12751. [[CrossRef](#)]
21. Bello, Y.H.; Ahmed, M.A.; Ookawara, S.; Elwardany, A.E. Numerical and experimental investigation on air distributor design of fluidized bed reactor of sawdust pyrolysis. *Energy* **2021**, *239*, 122179. [[CrossRef](#)]
22. Chladek, J.; Jayarathna, C.K.; Moldestad, B.M.; Tokheim, L.-A. Fluidized bed classification of particles of different size and density. *Chem. Eng. Sci.* **2018**, *177*, 151–162. [[CrossRef](#)]
23. Di Felice, R. Hydrodynamics of liquid fluidisation. *Chem. Eng. Sci.* **1995**, *50*, 1213–1245. [[CrossRef](#)]
24. Singh, P.; Mahanta, P.; Kalita, P. Numerical study on the gas-solid hydrodynamics and heat transfer in a rotating fluidized bed with static geometry dryer. *Int. J. Heat Mass Transf.* **2020**, *153*, 119666. [[CrossRef](#)]
25. Wang, L.; Wei, G.; Jiang, J.; Duan, S.; Xu, L.; Yuan, W.; Hou, Q. Experimental and Numerical Investigation of Particle Flow and Mixing Characteristics in an Internally Circulating Fluidized Bed. *J. Chem. Eng. Jpn.* **2019**, *52*, 89–98. [[CrossRef](#)]
26. DSouza, G.C. CFD Simulations of Bubble Column Equipped with Bundles of Concentric Tubes. Master’s Thesis, The University of Western Ontario, London, ON, Canada, 2020.
27. Jasim, M.M.; Mohammed, T.J.; Sabri, L.S. Air-lift Reactor’s Characterization via Computational Fluid Dynamic (CFD): Review. *Eng. Technol. J.* **2022**, *40*, 484–497. [[CrossRef](#)]
28. Chung, T.J. Computational Fluid Dynamics. *Br. J. Radiol.* **2009**, *82*. [[CrossRef](#)]
29. Bird, R.B.; Stewart, W.E.; Lightfoot, E.N. *Transport Phenomena*; John Wiley and Sons, Inc.: New York, NY, USA, 2002. [[CrossRef](#)]
30. Limtrakul, S.; Boonsrirat, A.; Vatanatham, T. DEM modeling and simulation of a catalytic gas–solid fluidized bed reactor: A spouted bed as a case study. *Chem. Eng. Sci.* **2004**, *59*, 5225–5231. [[CrossRef](#)]
31. Zhu, H.P.; Zhou, Z.Y.; Yang, R.Y.; Yu, A.B. Discrete particle simulation of particulate systems: Theoretical developments. *Chem. Eng. Sci.* **2007**, *62*, 3378–3396. [[CrossRef](#)]
32. Couderc, J.P. *Incipient Fluidization and Particulate Systems. Fluidization*, 2nd ed.; Academic Press: New York, NY, USA, 1985; pp. 1–44.
33. Lundberg, J.; Halvorsen, B.M. A review of some existing drag models describing the interaction between phases in a bubbling fluidized bed. In Proceedings of the 49th Scandinavian Conference on Simulation and Modeling, Oslo, Norway, 7–8 October 2008.
34. Syamlal, M.; O’Brien, T.J. Computer simulation of bubbles in a fluidized bed. *AIChE Symp. Ser.* **1989**, *85*, 22–31. [[CrossRef](#)]
35. Jasim, A.A.; Sultan, A.J.; Al-Dahhan, M.H. Impact of heat exchanging internals configurations on the gas holdup and bubble properties in a bubble column. *Int. J. Multiph. Flow* **2019**, *112*, 63–82. [[CrossRef](#)]
36. Li, T.; Grace, J.; Shadle, L.; Guenther, C. On the superficial gas velocity in deep gas–solids fluidized beds. *Chem. Eng. Sci.* **2011**, *66*, 5735–5738. [[CrossRef](#)]
37. Pare, A. *Hydrodynamics of Three Phase Fluidized Bed Using Low Density Particles*; Department of Chemical Engineering National Institute of Technology: Rourkela, India, 2013.

38. Irani, M.; Boozarjomehry, R.B.; Pishvaie, S.M.R.; Tavasoli, A. Investigating the effects of mass transfer and mixture non-ideality on multiphase flow hydrodynamics using CFD methods. *Iran. J. Chem. Chem. Eng.* **2010**, *29*, 51–60.
39. Sabri, L.S.; Sultan, A.J.; Al-Dahhan, M.H. Investigating the cross-sectional gas holdup distribution in a split internal-loop photobioreactor during microalgae culturing using a sophisticated computed tomography (CT) technique. *Chem. Eng. Res. Des.* **2019**, *149*, 13–33. [[CrossRef](#)]
40. Zhang, H.; Sun, Z.; Zhang, M.; Shao, Y.; Zhu, J. Comparison of the flow structures and regime transitions between a cylindrical fluidized bed and a square fluidized bed. *Powder Technol.* **2020**, *376*, 507–516. [[CrossRef](#)]
41. Sabri, L.S.; Sultan, A.J.; Majdi, H.S.; Jebur, S.K.; Al-Dahhan, M.H. A Detailed Hydrodynamic Study of the Split-Plate Airlift Reactor by Using Non-Invasive Gamma-Ray Techniques. *ChemEngineering* **2022**, *6*, 18. [[CrossRef](#)]
42. Sabri, L.S.; Sultan, A.J.; Al-Dahhan, M.H. Split internal-loop photobioreactor for *Scenedesmus* sp. microalgae: Culturing and hydrodynamics. *Chin. J. Chem. Eng.* **2021**, *33*, 236–248. [[CrossRef](#)]
43. Sabri, L.S.; Ojha, A.; Sultan, A.J.; Al-Dahhan, M.H. Integration of dynamic growth modeling and hydrodynamics in an internal-loop split photobioreactor. *J. Chem. Technol. Biotechnol.* **2022**, *97*, 1112–1127. [[CrossRef](#)]
44. Ojah, A.; Sabri, L.S.; Aldahhan, M.H. Local volumetric mass transfer coefficient estimation for *Scenedesmus* microalgae culture in a cylindrical airlift photobioreactor. *J. Chem. Technol. Biotechnol.* **2021**, *96*, 764–774. [[CrossRef](#)]
45. Pjontek, D.; Macchi, A. Hydrodynamic comparison of spherical and cylindrical particles in a gas–liquid–solid fluidized bed at elevated pressure and high gas holdup conditions. *Powder Technol.* **2014**, *253*, 657–676. [[CrossRef](#)]
46. Jin, H.; Lim, D.; Lim, H.; Kang, Y.; Jun, K.-W. Heat Transfer in a Liquid-Solid Circulating Fluidized Bed Reactor with Low Surface Tension Media. *Chin. J. Chem. Eng.* **2013**, *21*, 844–849. [[CrossRef](#)]
47. Taofeeq, H.; Al-Dahhan, M. Heat transfer and hydrodynamics in a gas-solid fluidized bed with vertical immersed internals. *Int. J. Heat Mass Transf.* **2018**, *122*, 229–251. [[CrossRef](#)]
48. Chalermssinsuwan, B.; Samruamphianskun, T.; Piumsomboon, P. Effect of operating parameters inside circulating fluidized bed reactor riser with ring baffles using CFD simulation and experimental design analysis. *Chem. Eng. Res. Des.* **2014**, *92*, 2479–2492. [[CrossRef](#)]
49. Yang, S.; Wan, Z.; Wang, S.; Wang, H. Computational fluid study of radial and axial segregation characteristics in a dual fluidized bed reactor system. *Energy* **2020**, *209*, 118359. [[CrossRef](#)]
50. Shi, W.; Yang, X.; Sommerfeld, M.; Yang, J.; Cai, X.; Li, G.; Zong, Y. Modelling of mass transfer for gas-liquid two-phase flow in bubble column reactor with a bubble breakage model considering bubble-induced turbulence. *Chem. Eng. J.* **2019**, *371*, 470–485. [[CrossRef](#)]